Geophysical Journal International

Geophys. J. Int. (2010) **183,** 1512–1524 doi: 10.1111/j.1365-246X.2010.04808.x

Quantifying potential tsunami hazard in the Puysegur subduction zone, south of New Zealand

Gavin P. Hayes[1,2] and Kevin P. Furlong[3]

[1] *U.S. Geological Survey National Earthquake Information Center, CO, USA. E-mail: ghayes@usgs.gov*
[2] *Synergetics Incorporated, Fort Collins, CO, USA*
[3] *Department of Geoscience, Pennsylvania State University, PA, USA*

Accepted 2010 September 10. Received 2010 September 4; in original form 2010 June 25

SUMMARY

Studies of subduction zone seismogenesis and tsunami potential, particularly of large subduction zones, have recently seen a resurgence after the great 2004 earthquake and tsunami offshore of Sumatra, yet these global studies have generally neglected the tsunami potential of small subduction zones such as the Puysegur subduction zone, south of New Zealand. Here, we study one such relatively small subduction zone by analysing the historical seismicity over the entire plate boundary region south of New Zealand, using these data to determine the seismic moment deficit of the subduction zone over the past ∼100 yr. Our calculations indicate unreleased moment equivalent to a magnitude M_w 8.3 earthquake, suggesting this subduction zone has the potential to host a great, tsunamigenic event. We model this tsunami hazard and find that a tsunami caused by a great earthquake on the Puysegur subduction zone would pose threats to the coasts of southern and western South Island, New Zealand, Tasmania and southeastern Australia, nearly 2000 km distant.

Key words: Tsunamis; Earthquake source observations; Seismicity and tectonics; Subduction zone processes; New Zealand.

1 INTRODUCTION

Subduction zone seismogenesis and tsunami potential have been a significant focus in modern geoscience literature (e.g. Lay *et al.* 1982; Pacheco *et al.* 1993; Tichelaar & Ruff 1993; Wells *et al.* 2003; Geist *et al.* 2006; McCaffrey 2008). The majority of these and other such studies focus on the hazards posed by major subduction zones, those with either a historic record of very large and/or tsunamigenic earthquakes, or with fault lengths and/or the extensive fault area necessary to host such an event in the future. Small subduction zones (e.g. Puysegur margin, south of New Zealand; the Lesser Antilles and South Sandwich Islands) have received relatively little attention (perhaps with the exception of the Hellenic Arc; e.g. Yolsal *et al.* 2007; Lorito *et al.* 2008), either because their tectonic history and present-day kinematics are uncertain, or perhaps because they were not thought capable of generating very large earthquakes because of their relatively small fault area.

Here we show that small subduction zones can pose significant earthquake and tsunami hazards, using the Puysegur Subduction Zone south of New Zealand as an example. The tectonic history of this margin is now well understood (e.g. Hayes *et al.* 2009) and the seismicity over the past ∼100 yr well documented at least for large earthquakes, making this location an ideal candidate for our analyses. This subduction zone is capable of hosting a megathrust earthquake and generating an associated tsunami that poses a hazard to the coasts of southern and western South Island, New Zealand, Tasmania and southeastern Australia, indicating that for this and other small subduction zones and subduction zone segments worldwide, such convergent margins cannot be discounted from generating large, hazardous events simply because of surface area and/or slow convergence rates.

2 PAST STUDIES OF THE PUYSEGUR SUBDUCTION ZONE

Evidence for a locked Puysegur subduction interface is described by Hayes *et al.* (2009). They use plate reconstructions of the Australian–Pacific Plate boundary south of New Zealand since 35 Ma, coupled with observations of high rates of intraplate seismicity within the Puysegur Block (Fig. 1) to suggest that substantial stresses internal to the Australian lithosphere outboard of the Puysegur subduction zone may be wholly or partially caused by the locking of the subduction interface.

The Puysegur subduction zone has also been identified as a potential tsunami hazard locally and regionally in studies by GNS Science in New Zealand (Berryman, 2005; Downes *et al.* 2005), and by researchers in Australia (Greenslade *et al.* 2007, 2009; Bathgate *et al.* 2008). Downes *et al.* (2005) report on two possible tsunamis in southwest New Zealand early in the 19th century, potentially related to earthquakes on the subduction interface (see online Supporting Information). These studies have modelled tsunamis resulting from

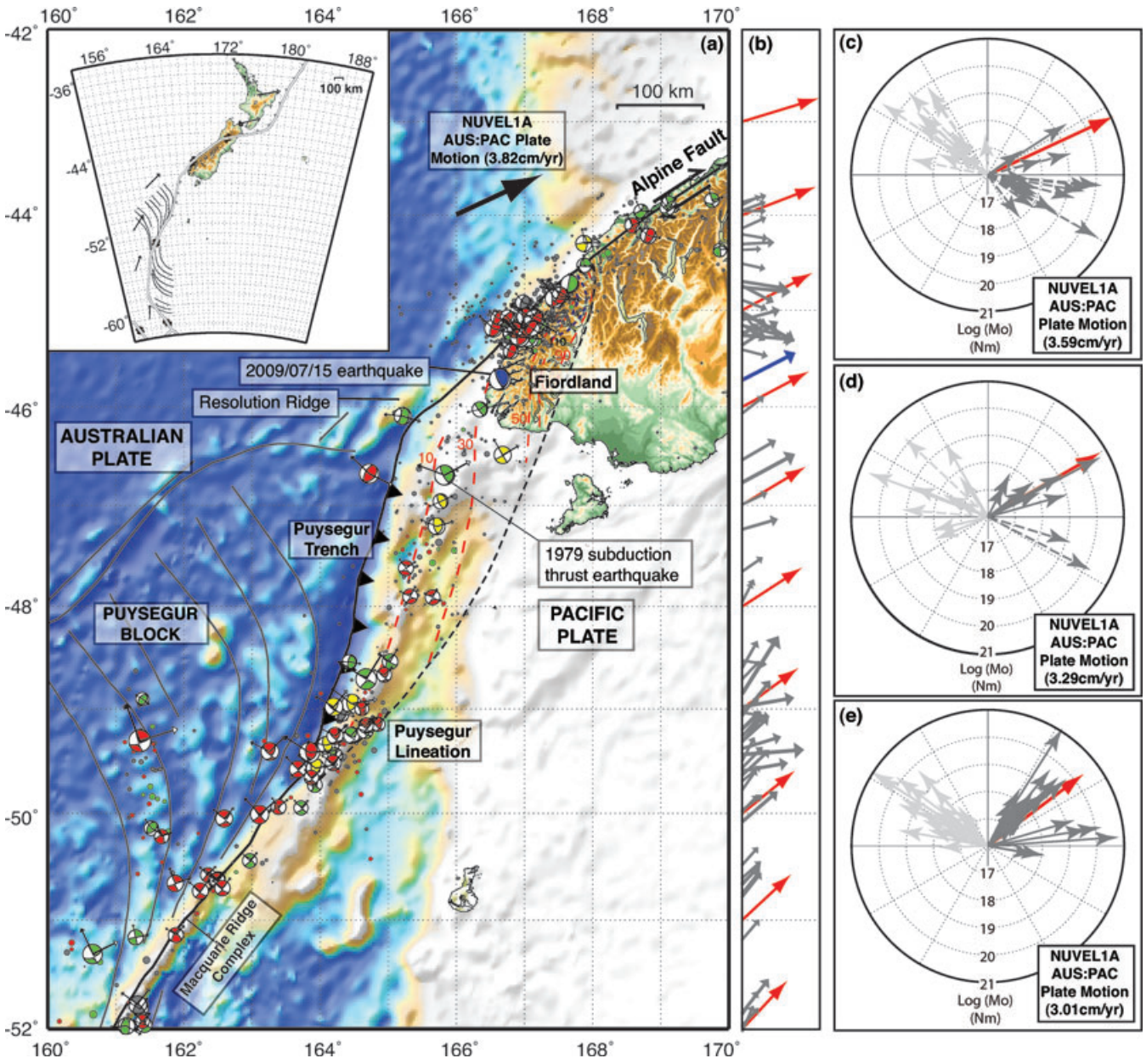

Figure 1. Present-day seismo-tectonics of the Australia–Pacific (AUS : PAC) plate boundary south of New Zealand. (a) Basemap. All major tectonic features are labelled. The plate boundary is shown in black; grey lines adjacent to the plate boundary south of New Zealand represent relic fracture zones from past periods of seafloor spreading. The black arrow at −44°S, 166°W represents the NUVEL1A (DeMets *et al.* 1994) derived plate motion at that location. Circles represent earthquake locations for events between 1973 and the present, scaled by magnitude. Centroid Moment Tensor solutions (CMTs), also scaled by magnitude, are shown where they exist. Earthquakes locations are plotted according to the following (highest to lowest) hierarchy: (1) relocations (Hayes *et al.* 2009) using the methodology of Ammon (2004) in red; (2) relocations from the EHB catalogue (Engdahl *et al.* 1998) in green; (3) locations provided by Moore *et al.* (2002) in yellow and (4) U.S. Geological Survey National Earthquake Information Center (USGS, NEIC) locations, in dark grey. Location of the 1979 event used for subsequent tsunami modelling is labelled. Blue mechanism corresponds to the 2009 July 15 M_w 7.8 earthquake. Contours of the Benioff zone are shown in red dashed lines between 10 and 90 km, and blue dashed lines between 110 and 130 km. Inset shows the regional tectonics of the AUS : PAC plate boundary surrounding New Zealand. Plate motions of Australia relative to a fixed Pacific from NUVEL1A are shown with grey arrows. (b) The variation of earthquake slip vectors with latitude along and east of the AUS : PAC plate boundary. For simplicity, we plot the slip vector for each earthquake that is most closely aligned with plate motion (not necessarily the fault plane). Slip vectors are shown as grey arrows, whose length corresponds to earthquake magnitude. Red arrows represent the plate motion at the plate boundary at that latitude. Blue arrow represents the slip vector of the 2009 July 15 earthquake. (c)–(e) Shown are rose diagrams of these slip vectors, in dark grey, and slip vectors corresponding to slip on the auxiliary plane, in light grey, plotted with the NUVEL1A (DeMets *et al.* 1994) AUS : PAC plate motion at that location, for three areas along the plate boundary—the Fiordland earthquake sequence (at the transition from Puysegur subduction to Alpine Fault translation), in (c); within the Puysegur subduction zone itself, in (d); and at the Puysegur Lineation (at the southern transition from Macquarie Ridge translation to Puysegur subduction), shown in (e). Where slip vectors are dashed, earthquakes are inferred to be intraplate events, likely resulting from slip on the auxiliary (light grey) plane. Within the Puysegur subduction regime, virtually all earthquake slip vectors are consistent with Australia–Pacific plate motions. At the two transitions there is a mixture of two slip-vector orientations—those in the plate motion direction, and those perpendicular to the plate boundary orientation.

great earthquakes along this margin, incorporating their results into hazard response efforts in each country. However, the studies in question use earthquake scenarios with no specific physical basis—either using a range of magnitudes to simulate generic worst-case scenario models at all regional subduction zones (Greenslade *et al.* 2007, 2009), or calculating maximum magnitude based on plate boundary length (Berryman, 2005; Downes *et al.* 2005), inappropriate in subduction zone environments where margin length is often unrelated to earthquake potential (note that in their calculations of empirical relationships between earthquake size and fault parameters, Wells & Coppersmith (1994) excluded subduction zone earthquakes). These studies are thus not based on the Puysegur subduction itself, but rather impose scenarios to model resulting tsunami processes. Furthermore, some of these studies used incorrect source geometry for the Puysegur margin (Greenslade *et al.* 2007, 2009), dipping west rather than east, as acknowledged in Greenslade *et al.* (2007). Some of these studies (Berryman 2005; Downes *et al.* 2005) also failed to take into account the oblique nature of subduction (Fig. 1) and the impact of such obliquity on earthquake slip and tsunami-wave generation and propagation. This obliquity of motion means slip on a broad and shallow thrust interface will be oriented approximately normal to the New Zealand coastline (i.e. NE–SW), rather than occurring on a steep fault nearly parallel to it (E–W), altering hazard both from shaking and from tsunamis. Finally, these studies treated the Puysegur subduction zone in two segments; a northern section offshore Fiordland, and a southern section south of the Resolution Ridge. There is no evidence for such segmentation (there having been no great historic ruptures terminating at, or crossing such a boundary), and as it is unclear what role the Resolution Ridge plays in subduction (lying beyond the western limit of subduction on the upper plate), we treat the Puysegur subduction zone as one complete segment. By building on our current understanding of the tectonic setting of this margin (Hayes *et al.* 2009), and by specifically quantifying past earthquake activity and future earthquake potential, we provide an earthquake scenario with realistic constraints, and thus a physical basis for the potential hazard of the Puysegur subduction zone.

3 TECTONIC SETTING OF THE PUYSEGUR SUBDUCTION ZONE

Relative plate motion between the Australian (AUS) and Pacific (PAC) plates between approximately 45°S and 50°S is accommodated via oblique convergence at the Puysegur trench (Fig. 1), where oceanic crust of the Australian Plate has been subducting beneath the southwest corner of New Zealand, on the PAC Plate, since approximately 20 Ma (Lebrun *et al.* 2003). At either end of the Puysegur trench, the plate boundary changes from subduction to translational faulting, accommodating oblique strike-slip motion along the Macquarie Ridge Complex (MRC) to the south and the Alpine Fault (AF) to the north.

To the north, the Alpine Fault marks the main plate boundary structure to the South Island of New Zealand (Fig. 1, inset). Along much of the length of the Alpine Fault, plate motions are transpressional, resulting in the uplift of the Southern Alps. South of the Puysegur trench, AUS : PAC motion is translational (right-lateral) along the MRC (Fig. 1). Between ∼40–25 Ma, this system was dominantly divergent, hosting seafloor spreading at the Macquarie Spreading Center (Cande & Stock 2004; Hayes *et al.* 2009). Since that time, major changes in the AUS : PAC motions, seen in the rapid southward migration of the AUS : PAC Euler Pole, led to reorganizations along the margin that have generated the structure we see today, leading to subduction initiation of the Australian Plate at the Puysegur trench (Fig. 1).

These rapid spatial and temporal changes in plate boundary structure and convergence obliquity have resulted in a complex tectonic regime. Previously, some authors have argued that subduction occurs in a west-to-east direction normal to the trench, where the Australian Plate bends over rapidly after subduction, and slip partitioning occurs in the overlying plate to balance plate motions (e.g. Reyners *et al.* 2002; Sutherland *et al.* 2006). Our results indicate a plate tectonic system with gently dipping subduction towards the northeast, which satisfies plate motion and is more consistent with the slip vectors of historic earthquakes in the region (Fig. 1, Section 4.1), can match Benioff-zone structure and is required to match the high gravity and topography observed in Fiordland directly above the subducting plate (Lebrun *et al.* 2003; Malservisi *et al.* 2003). We build on recent tectonic models of this plate boundary by Hayes *et al.* (2009) that place modern-day observations of seismicity and plate tectonics into an evolutionary context to resolve these differences, showing seismicity on and around this plate boundary today is best explained through oblique subduction at the Puysegur trench, and assess the implications for seismo- and tsunami-genesis.

4 REGIONAL SEISMICITY

Between 1990 January and 2009 May, over 750 earthquakes with $M \geq 5$ occurred in the plate boundary region between 44°S and 52°S [U.S. Geological Survey National Earthquake Information Center (USGS NEIC) Preliminary Determination of Epicentres (PDE); centennial catalogue of Engdahl & Villesenor 2002], encompassing the Puysegur subduction zone and its transitions to translational faulting (Fig. 1), including 16 events with $M \geq 7$ and two events with $M \geq 8$. Despite high rates of seismicity to the south of the Puysegur subduction zone along the MRC, within the adjacent Australian oceanic lithosphere (a region termed the Puysegur Block by Hayes *et al.* 2009), at the southern transition from translational motion along the MRC to subduction, and at the northern transition from subduction to translational motion along the Alpine Fault, seismicity rates remain low in the Puysegur subduction zone itself (Figs 1 and 2). In fact, in this period (up to 2009 May) there have been only three known earthquakes ($M > \sim 5.5$) with thrust mechanisms indicative of subduction within the subduction zone south of mainland South Island, the largest of which was an M_w 7.3 event in 1979. An M_w 7.1 event occurred in 2004 November outboard of the subduction zone; an event which was incorrectly located within the subduction zone in the GNS earthquake catalogue, but the relocated catalogue of Engdahl *et al.* (1998, and catalogue updates; hereafter labelled EHB) confirm its location outside the trench. Detailed analyses from local studies reveal two strike-slip earthquakes in the Puysegur region over this time period that occurred on shallow upper-plate translational structures rather than on the subduction interface itself (Downes *et al.* 2005). Other studies (Doser *et al.* 1999) in the Fiordland region near the northern transition from subduction to translational motion identified historical earthquakes that were interpreted to reflect internal deformation of the subducting Australian slab. A sequence of large thrust earthquakes also occurred near this transition beneath and offshore of western Fiordland over the past ∼30 yr, which we and others (Lebrun *et al.* 2003; Malservisi *et al.* 2003; Hayes *et al.* 2008) interpret as intraplate tearing events within the Australian Plate, rather than being interplate subduction interface earthquakes (e.g. Reyners *et al.*

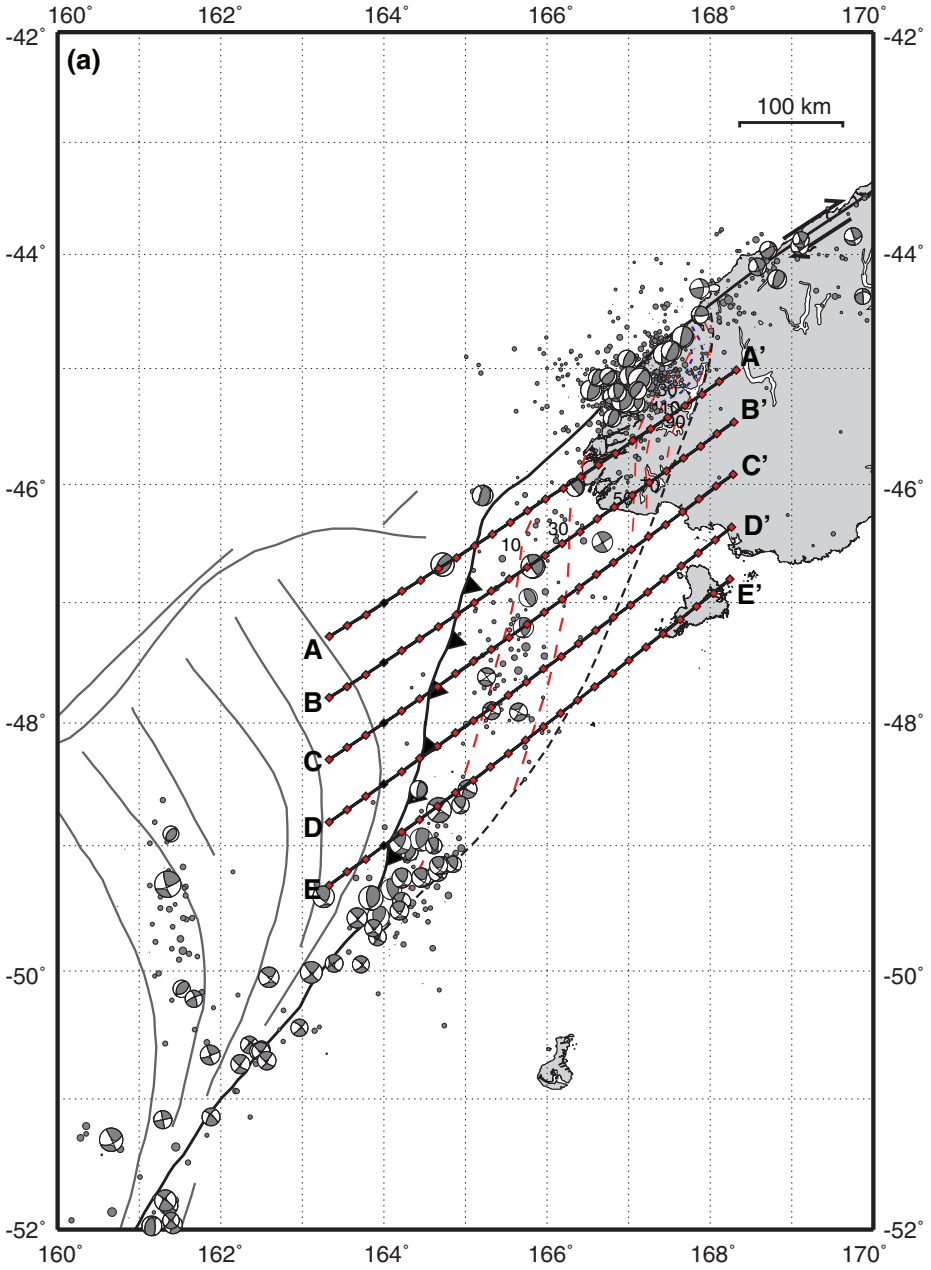

Figure 2. Cross-sections through the Puysegur subduction zone. Sections made in the direction of plate motion. (a) The locations of profiles (A, C, E) are shown in the basemap. (b) In each cross-section (A, C, E), seismicity within ±50 km of each profile is projected. Dark grey circles represent earthquake locations for events between 1973 and the present from the EHB and PDE catalogues, white circles events over the same time period from the catalogue of GNS Science, New Zealand. CMTs shown in Fig. 1 are also projected onto the cross-sections, viewed from the southeast. The blue dashed line on each section represents the projection of Benioff zone contours onto the profile. In cross-section A, we also show the width of each Benioff-Zone contour obliquely projected onto the section (horizontal red dashed lines), and associated upper and lower bounds to the surface of the 3-D slab (thin blue dot–dashed lines) projected onto the 2-D section.

2002; McGinty & Robinson 2007*)*. This interpretation is consistent with analyses of slip vectors of earthquakes in Fiordland (Fig. 1 and Section 4.1); cross-sections of the sparse seismicity within the subduction zone (Fig. 2) show that a shallowly dipping, northeast-oriented Benioff zone is fully compatible with the distribution of earthquakes in this region. This interpretation is also consistent with the location and mechanism of an approximate M_w 7.8 earthquake that occurred to the southwest of Fiordland in 2009 July, an event discussed in detail in Section 4.2.

The total moment release of these three Puysegur subduction-related events is approximately 1.2×10^{20} Nm. Increasing this figure by 10–20 per cent to account for moment release from smaller earthquakes 'missing' from our record (Bilham & Ambraseys 2005) gives a total released moment of approximately 1.4×10^{20} Nm. Over the same time period, this subduction zone has experienced plate motion equivalent to a seismic moment release of approximately 4.0×10^{21} Nm, based on an average plate motion of 3.5 cm yr^{-1} and assuming a shallow seismogenic interface surface area of

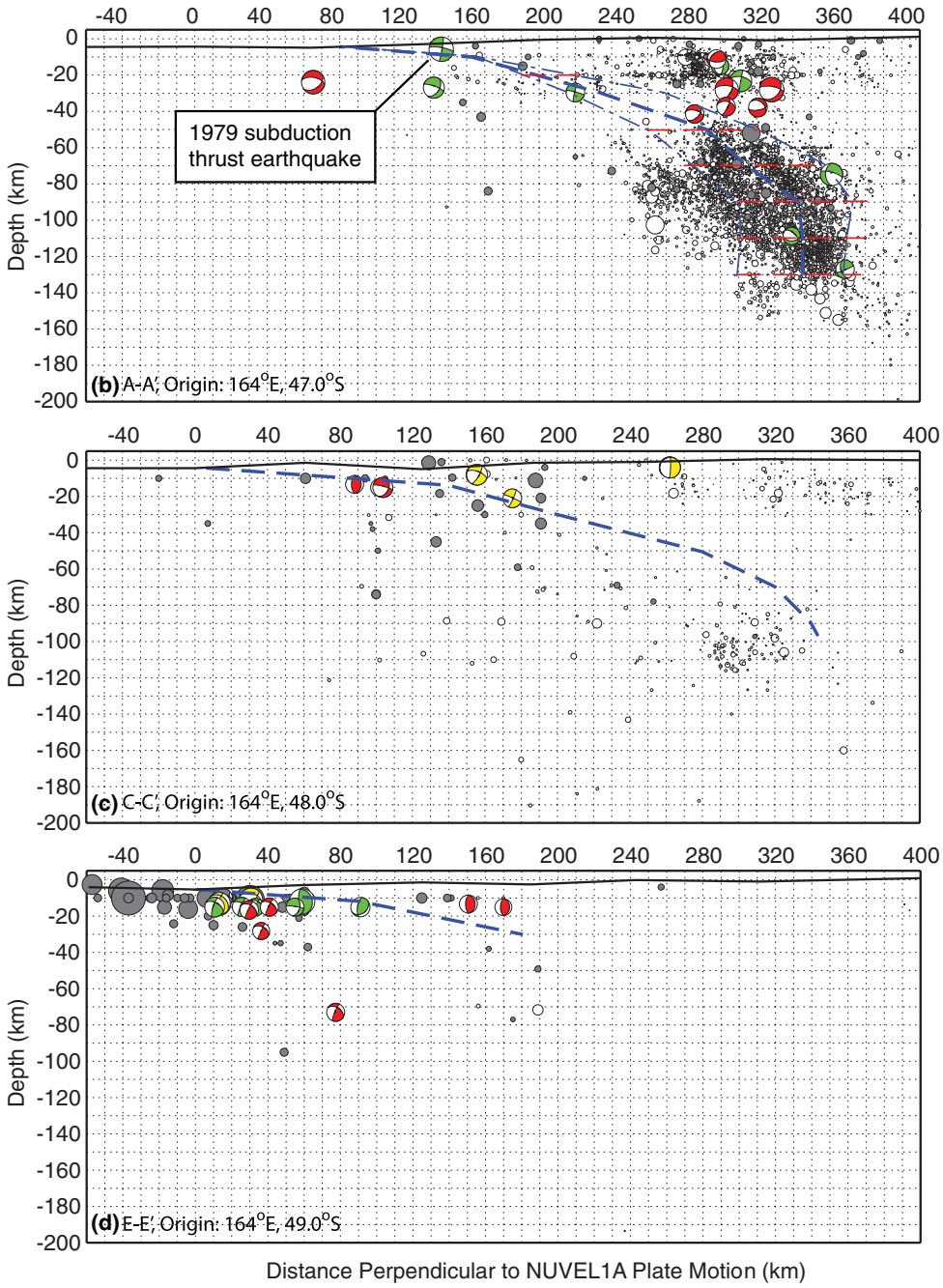

Figure 2. (*Continued.*)

3.5×10^4 km^2 and a relatively low shear modulus of $\mu = 30$ GPa (e.g. Hayes *et al.* 2009).

The ratio of observed moment release to moment potential calculated from accumulated motion gives a measure of apparent seismic coupling (Peterson & Seno 1984; Pacheco *et al.* 1993), α, and suggests a value of 0.04. Such a low ratio can mean one of two things—either much of the motion at this subduction zone is accommodated aseismically, or the sampled period was too short to capture the characteristic seismic behaviour of the interface. In the first case, great earthquakes probably will not occur (e.g. Marianas-type subduction; Lay *et al.* 1982). In the second case, having only analysed a short earthquake record, such a low ratio more likely means that we have not sampled a selection of seismicity representative of the earthquake cycle at this subduction zone, and great earthquakes that accommodate the 'missing' moment are possible (as are many smaller magnitude events). We note that in Pacheco *et al.* (1993) the Sumatra subduction zone had a calculated 90-yr coupling of $\alpha = 0.07$. If all motion at the Puysegur subduction zone is accommodated seismically (i.e. a seismic coupling ratio of one), the missing moment we have calculated equates to a slip deficit with a moment equivalent of 3.8×10^{21} Nm—equivalent to an earthquake of M_w 8.3.

Given repeat rates of great earthquakes on the order of 100 yr or more at many global subduction zones (Pacheco *et al.* 1993), the hazard suggested by these calculations is significant. Such calculations assume that all of the accumulated moment can be released

seismically in one event, and as such describe a worst-case scenario, but nevertheless they allow us to quantify the potential hazard posed by this subduction zone. We note that even if just 50 per cent of this moment deficit were released seismically in one event, an earthquake of M_w 8.1 would be generated.

4.1 Slip vector analysis

We place Puysegur seismicity into a regional context by analysing earthquakes within the subduction zone in conjunction with seismicity occurring in the surrounding lithosphere. By analysing earthquakes at the subduction transitions surrounding Puysegur, we can infer if and how the convergence direction of the subducting plate changes over the length of its' boundary (Fig. 1), and thus which historic events are likely to represent subduction-related motion, and what direction of motion we can expect for future events. Results show a mixture of plate-motion-oriented events and highly oblique events at the southern transition; events nearly perpendicular to plate motion at the northern transition, with a few plate-motion-oriented shallow thrusts; and dominantly plate-motion oriented events in the Puysegur subduction zone itself. These patterns lead to two major observations:

(i) Slip partitioning is an unlikely candidate for explaining the obliquity of earthquake slip in Fiordland, as further south within the Puysegur subduction zone events are well aligned with plate motion (Fig. 1). Furthermore, there is no likely candidate fault onto which slip can be partitioned (such a fault must be east of oblique slip earthquakes; Fig. S1). The fact that the majority of earthquake slip vectors here are highly oblique to plate motion directions, coupled with the lack of evidence for a structure onto which motion could be partitioned if these events were subduction related, lead us to agree with the interpretations of others (e.g. Lebrun *et al.* 2003; Malservisi *et al.* 2003; Hayes *et al.* 2009) that these events do not represent AUS : PAC subduction interface earthquakes in this region.

(ii) Within the shallow portion of the Puysegur subduction zone itself, seismic slip is aligned with plate motion, supporting our inference that the Australian Plate subducts in a direction aligned with plate motion. Only two events in this region have slip vectors oblique to the plate motion direction (Fig. 1d), and both of these events are located *outboard* of the subduction zone (an M_w 7.1 event in 2004, and the Resolution Ridge M_w 6.2 earthquake in 1985 January). Their locations southwest of the large cluster of thrust events in and offshore Fiordland, in a direction parallel to plate motion from those earthquakes, and the similarity of mechanisms and slip vectors with those earthquakes, support the conclusions of Malservisi *et al.* (2003), Lebrun *et al.* (2003) and Hayes *et al.* (2009) that some or all of these earthquakes may represent tearing within the Australian Plate, decoupling the bulk of the plate that translates past the South Island of New Zealand along the Alpine Fault from the subducting slab.

4.2 2009 July 15 M_w 7.8 earthquake

On 2009 July 15, an approximate M_w 7.8 earthquake occurred near the southwestern coast of Fiordland (global centroid moment tensor project (gCMT); http://globalcmt.org), where Benioff-zone structure of the subducting Australian Plate begins its transition from a northeastward, shallowly dipping plane to a more complex, deformed and steeply dipping structure beneath Fiordland itself (Fig. 1).

This earthquake is particularly relevant in the context of regional tectonics and seismicity discussed above. The location of the event is approximately 100 km to the south of the large cluster of earthquakes offshore of western Fiordland (Fig. 1), which we associate with tearing within the Australian Plate. The gCMT solution for the event indicates shallow thrust faulting beneath Fiordland, South Island New Zealand (strike $\phi = 26^\circ$, dip $\delta = 24^\circ$, rake $\lambda = 140^\circ$, moment $m_0 = 6.0 \times 10^{20}$ Nm). Similar results were obtained by CMT ($\phi = 27^\circ$, $\delta = 33^\circ$, $\lambda = 126^\circ$, $m_0 = 3.1 \times 10^{20}$ Nm) and W-phase ($\phi = 18^\circ$, $\delta = 23^\circ$, $\lambda = 123^\circ$, $m_0 = 4.3 \times 10^{20}$ Nm) inversions at the USGS NEIC. These three solutions imply slip vectors of 63°, 76° and 72°, respectively; Nuvel1A plate motion at the epicentre of the earthquake is oriented towards 64°. The depths of these solutions range from 19 to 25 km. Initial estimates of the earthquake depth by the NEIC ranged between 25 and 35 km, but are poorly resolved due to the emergent nature of the event. Modelling of the main shock and several aftershocks using short-period regional body waves suggest depths between 20 and 30 km. The alignment between earthquake slip and plate motions, and the consistency between the hypocentre and slab depth as indicated by Benioff-zone contours for the subducting Australian Plate (Fig. 1) suggest that the event likely occurred on the subduction interface, releasing a small fraction of the plate-motion-related moment deficit calculated in Section 4. Based on these depth estimates, we fix the depth of the main shock hypocentre at 25 km in subsequent analyses, consistent with the depth of the slab interface at the epicentre (Fig. 1).

We invert for the rupture model of the earthquake using broadband teleseismic *P* and *SH* body waveforms, and long period surface waves recorded at Global Seismic Network stations worldwide. Data were selected based upon quality (high signal-to-noise ratios) and azimuthal distribution. Waveforms are first converted to displacement by removing the instrument response and then used to constrain the slip history based on the finite fault inversion algorithm of Ji *et al.* (2002). Although we model slip on both planes of the gCMT solution, comparisons between data and synthetics indicate the shallow, east-dipping plane is preferred. Our inversion recovers approximately 86 per cent of the teleseismic data signal. Results (Fig. 3) show the majority of slip during the earthquake was located west and slightly to the south of the hypocentre (i.e. updip), in agreement with the relative locations of the hypocentre and CMT centroid locations, which represent the earthquake nucleation and approximate average slip locations, respectively. Similar rupture models are obtained using each CMT solution discussed above, indicating the robustness of the locus of major slip. In our preferred model (Fig. 3), peak slip is ~5.5 m, and the total moment release 6.0×10^{20} Nm, identical to the gCMT solution. The source time function for the earthquake (Fig. 3c) indicates fairly rapid moment release after an emergent onset, concentrated between 5 and 30 s after the event origin time.

This earthquake is the largest known Puysegur-subduction-related earthquake to date. Seismic moment release during the event was approximately 6.0×10^{20} Nm, implying an adjusted seismic coupling coefficient for this subduction zone of $\alpha = 0.19$. This scale of energy release does not significantly reduce the seismic moment deficit calculated for the Puysegur subduction zone (~3.8×10^{21} Nm versus ~3.3×10^{21} Nm, still equivalent to an earthquake of M_w 8.3). However, the event does highlight the hazard of this subduction zone; scaling the moment release of this event by the ratio of the area of the shallow thrust interface to the area that slipped during this earthquake implies a moment of 3.5×10^{21} Nm, supporting our analyses for an earthquake

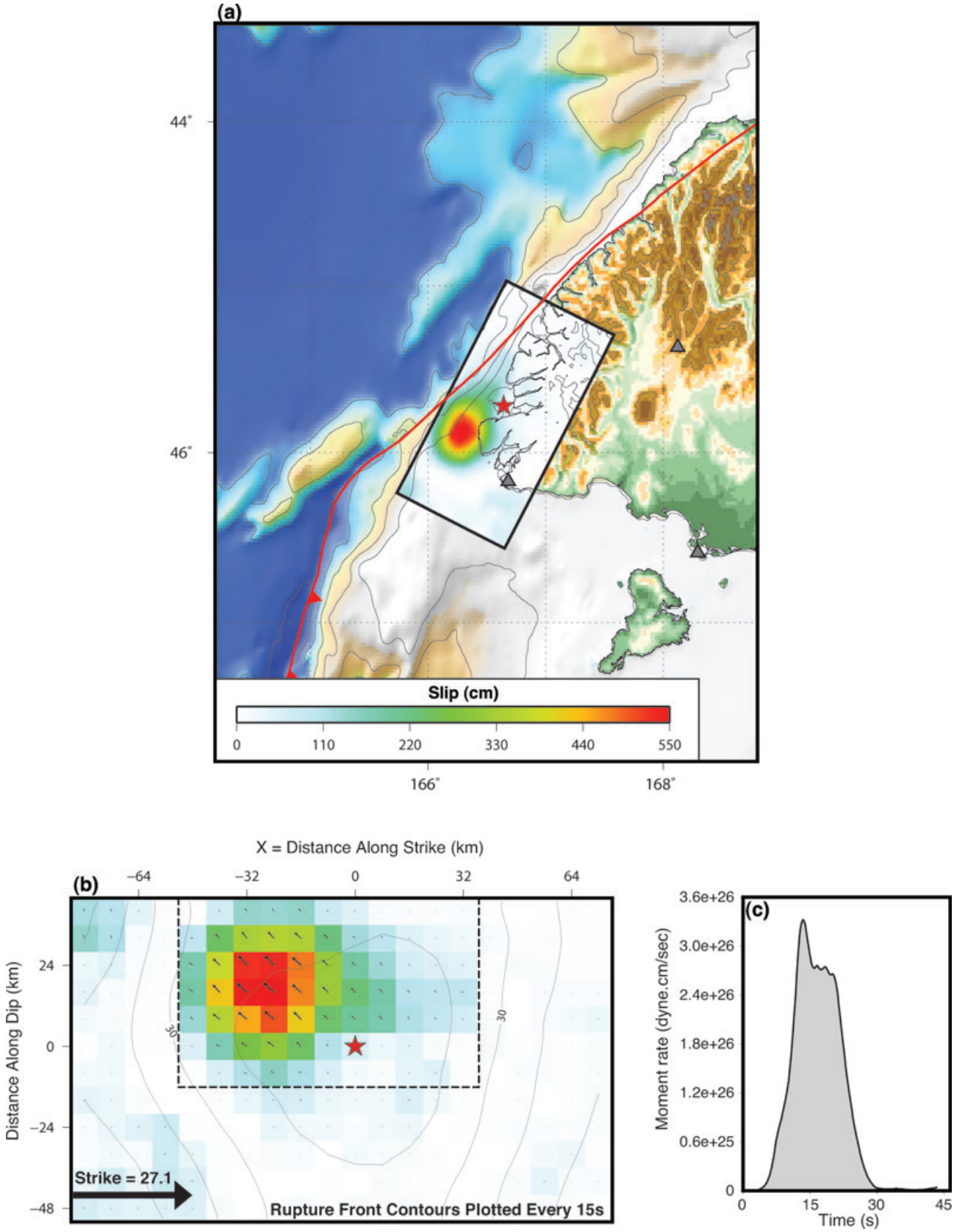

Figure 3. Coseismic slip distribution for the 2009 July 15 earthquake. (a) Surface projection of the coseismic slip distribution, calculated through analysis of 15 teleseismic broad-band *P* and 15 broad-band *SH* waveforms, and 31 long period surface waves. The inversion models slip on the shallow, east-dipping fault plane of the gCMT solution, shifted to the initial hypocentre of the NEIC (red star; 166.64, –45.72). (b) Fault plane reference frame view of coseismic slip distribution and temporal evolution of slip. Rupture front contours are plotted every 15 s. The black dashed line outlines the area of major slip during the earthquake, used for modelling uplift and tsunami propagation. (c) Source time function, describing the rate of moment release with time.

generated by slip over the entire shallow surface area of the fault.

5 PUYSEGUR TSUNAMI HAZARD

5.1 2009 July 15 tsunami

Before analysing tsunami potential from future earthquakes in this subduction zone, we first model the tsunami generated by the 2009 July M_w 7.8 event, and use this as a benchmark test of our approach and methodology. For our tsunami calculations we use the GeoClaw routines of the Clawpack 5.0 software package (http://www.amath.washington.edu/~claw/), which uses a finite volume approach to solve non-linear hyperbolic shallow water equations on a grid of varying resolution. The tsunami is modelled over an initial 100 × 100 cell grid, each approximately 40 km × 40 km, with the dynamic refinement capabilities of the GeoClaw package employed in deep water up to a factor of ×8 (i.e. ~5 km^2 cells), and in shallow water (<1000 m) and the region of the ruptured fault to a factor of ×64 (i.e. ~0.5 km^2 cells). We do not model tsunami run-up in very shallow water at the coastlines, instead focusing on tsunami behaviour offshore. The GEBCO_08 grid (version 20091120, http://www.gebco.net) is used for the bathymetry model.

Combining the slip inversion discussed in the previous section to generate sea-surface displacement (Fig. S2) and the methodology discussed above, we model the propagation and amplitude of the resulting tsunami, comparing our calculations with the tsunami observations made by the Pacific Tsunami Warning Center (PTWC; http://www.prh.noaa.gov/ptwc/) and archived at the National Data Buoy Center (NDBC; http://www.ndbc.noaa.gov/). In the open waters of the Tasman Sea, a DART buoy (Tasman Sea Station 55015) measured a 5-cm tsunami with a period of 8 min and 31 min after the origin time of the earthquake. For reference, this location is marked on Fig. 4. Tsunami modelling results (Fig. 4) show that this open sea observation can be reproduced extremely well, matching the amplitude, period and timing within a few millimetres and several minutes. The reproducibility of tsunami observations for this earthquake lend confidence in our ability to model a larger, scenario earthquake on the Puysegur subduction zone, allowing us to better evaluate the potential tsunami hazard for this region.

5.2 Puysegur tsunami hazard

To model the tsunami hazard for possible future great earthquakes in the Puysegur subduction zone, we have created a 'scenario' event based on the location of the 1979 M 7.3 earthquake on the subduction interface, with a magnitude given by the moment deficit determined by slip accumulation over the past >100 yr and moment release during earthquakes over the same time period (Section 4). Using the focal mechanism of the 1979 event (Fig. 1), we construct a fault plane that includes the entire shallow section of the subduction thrust interface (Fig. 5a, Table 1). As these planes dip in a direction oblique to plate motion, we simulate plate motion directed slip by setting a rake angle for the scenario event of 036°. We calculate the expected uplift of the seafloor during the event using the Coulomb 3.1 package (Lin & Stein 2004; Toda *et al.* 2005; Fig. 5b), providing a model of static displacements resulting from the motion of a fault in an elastic half-space. The slip specified on the fault primarily displaces the upper plate in this model.

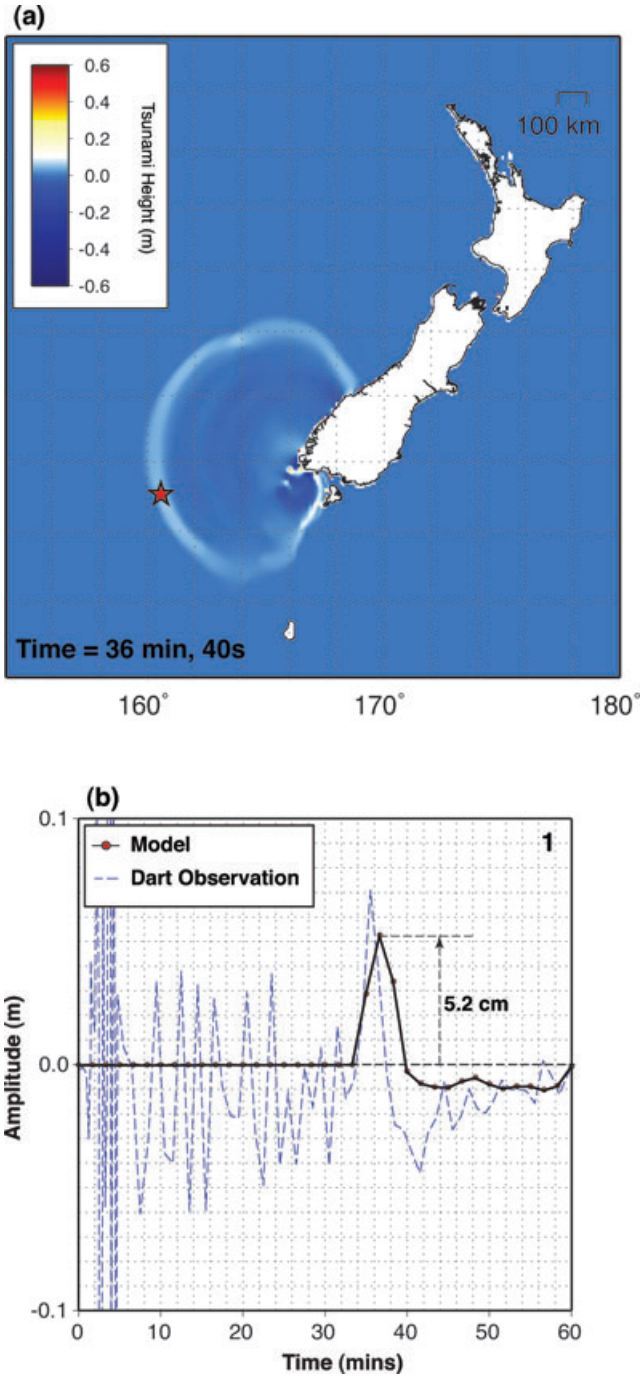

Figure 4. Tsunami calculations for the 2009 July 15 earthquake. (a) Tsunami amplitude 36 min after initiation, approximately when the modelled tsunami arrives at the site of the Tasman Sea DART buoy (Station 55015) where the tsunami caused by the earthquake was observed. (b) Modelled tsunami time-series at the Tasman Sea Dart buoy [red star in (a)].

Using the same approach discussed in Section 5.1, we model potential tsunami propagation from our scenario earthquake to calculate the approximate timing and open water heights of such a tsunami. The arrival times of the first increase in water level are shown in Fig. 6. Fig. 7 shows a snapshot of the tsunami 30 min after the initial seafloor uplift. These results indicate that a tsunami caused by a great earthquake on the Puysegur subduction zone poses a threat to the southern and western coasts of the South Island of

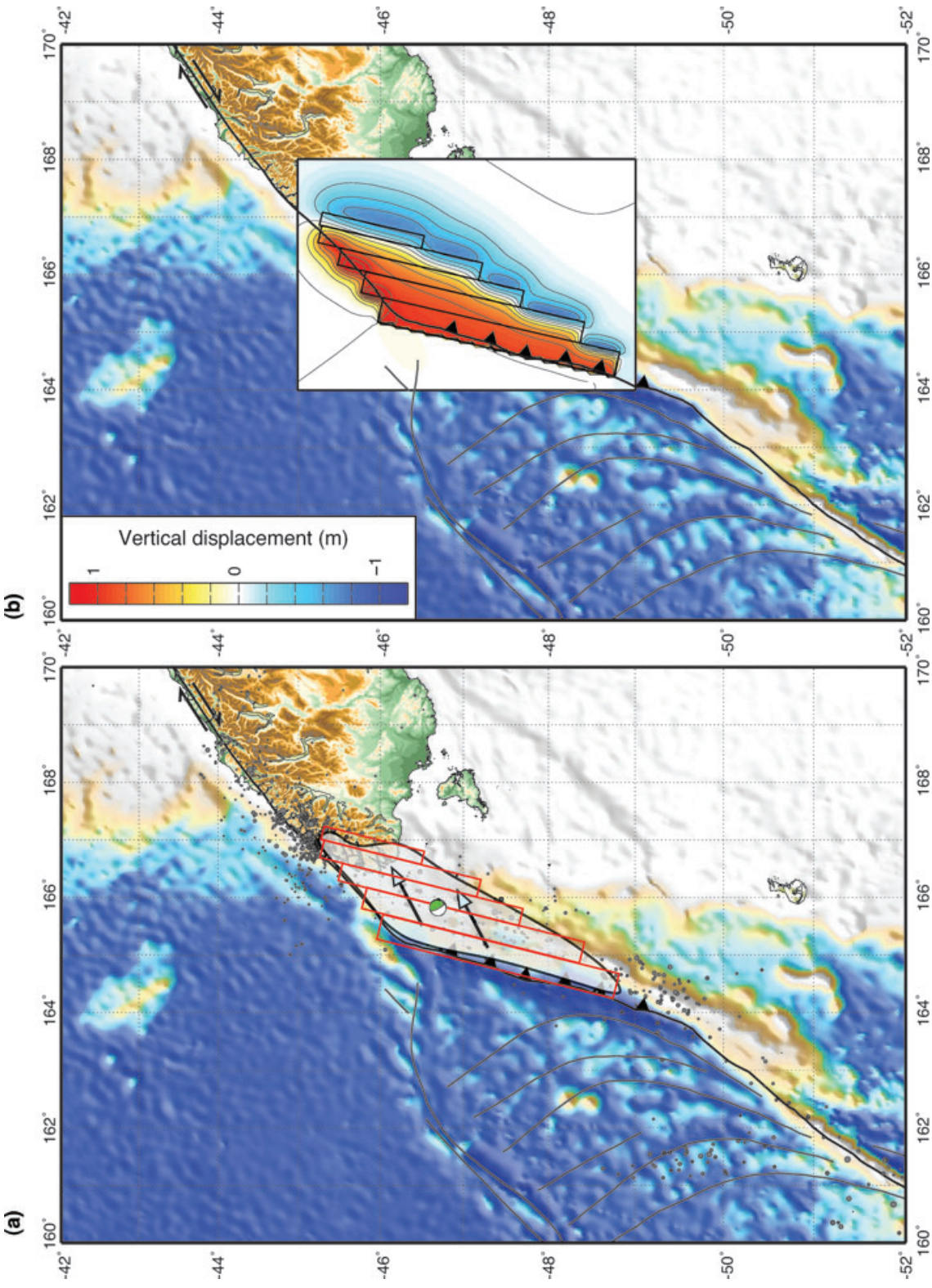

Figure 5. Scenario earthquake rupture model used to generate a tsunami. (a) Potential rupture area (white) for a Puysegur trench megathrust earthquake, assuming that almost the entire shallow-dipping portion of the thrust interface slips in one event, a shear modulus for oceanic crust of $\mu = 30$ GPa, and an average slip of $d \sim 4$ m, corresponding to a seismic moment of $m_o \sim 3.8 \times 10^{21}$ Nm ($M_w \sim 8.3$). Overlain in red, fault geometry and hypocentral location of the scenario event, modelled on the location and mechanism of the 1979 interplate thrust earthquake. We divide the seismogenic zone into five rectangular fault segments to account for the change in width of the thrust interface (due to the obliqueness of subduction), each dipping 13° (the dip of the shallow plane of the 1979 event). See Table 1 for fault parameters. (b) Resulting uplift from such an earthquake, modelled using Coulomb 3.1 (Lin & Stein 2004; Toda *et al.* 2005). Uplift contoured every 20 cm. The relation between fault slip (moment) and absolute uplift will also depend on the partitioning of slip across the megathrust during an event (Furlong *et al.* 2009).

Table 1. Fault parameters used to model sea-surface uplift resulting from our scenario earthquake. Each fault plane is defined using Cartesian coordinates embedded in a lat/lon grid, with bounds −49.0 to −45.0, 164.0 – 168.0. Fault parameters used were $\phi = 19^\circ$, $\delta = 13.5^\circ$, $\lambda = 144^\circ$, with 4 m of slip on each segment. The depth of each segment (Z-Top) is referenced to the average ocean depth over the modelled grid.

Fault ID	X-Start (km)	Y-Start (km)	X-Finish (km)	Y-Finish (km)	Z-Top (km)	Z-Base (km)
Puy1	−128.35	−196.02	−56.44	115.38	0.0	8.0
Puy2	−83.76	−151.04	−17.25	137.25	8.0	14.8
Puy3	−36.5	−72.25	19.50	168.00	14.8	20.2
Puy4	−0.65	−17.60	49.00	194.00	20.2	25.8
Puy5	41.00	57.75	72.00	192.00	25.8	30.0

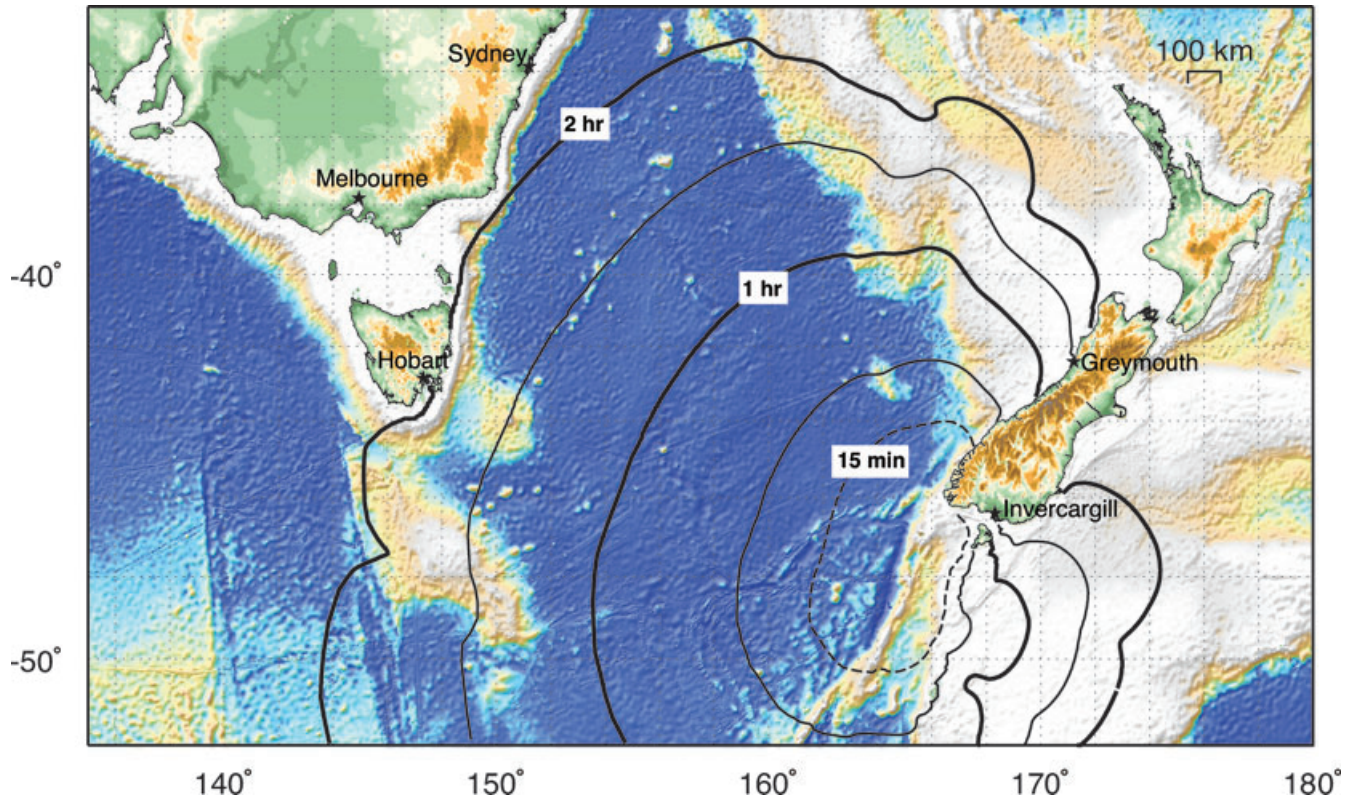

Figure 6. Tsunami model for earthquake scenario. Plot shows the arrival time of the first increase in water level. Contour interval is 30 min, with an additional contour shown 15 min after initiation. Arrival times are overlain on a map of seafloor bathymetry (GEBCO_08, http://www.gebco.net/). Major cities in New Zealand and Australia are labelled and starred for reference.

New Zealand, the coasts of Tasmania, and also to the southeastern coast of Australia, nearly 2000 km distant. Maximum open-ocean water heights dissipate away from the ruptured fault to <1 m at distances of ∼100 km. The tsunami rapidly approaches the Fiordland coast with open-ocean heights between 0.5 and 0.8 m, making landfall in less than 15 min (see video animation in online Supporting Information). Heights fall-off rapidly near the southwest tip of Fiordland, and the tsunami moves slowly up the west coast of the South Island with open-ocean heights between 0.1 and 0.2 m, reaching Greymouth in ∼1.5 h. Moving east from the epicentre, the tsunami dissipates over the shallow water of the continental shelf. Tsunami heights approaching Stewart Island are ∼0.5 m, but lose amplitude as they travel slowly past the island and drop to less than 0.1 m as they traverse the east coast of the South Island. Open-ocean heights near Invercargill on the southeast coast of the South Island are between 0.1 and 0.3 m. The resolution of this model does not account for the effects of edge waves, a trapped tsunami mode in the near-shore which travel slower and often with greater amplitudes than the tsunami mode modelled here (González *et al.* 1995); our estimates thus act as a lower bound on expected deep-water tsunami heights for the modelled earthquake.

Moving west towards Australia, the tsunami retains heights >0.2 m over the deep ocean. Approaching Tasmania, the tsunami grows to ∼0.3 m in the open-ocean and reaches land in ∼2 hr (see video animation in online Supporting Information). Tsunami heights could be much higher at the shoreline due to amplification factors of ×2 or more caused by local bathymetry (Kajiura 1986; Power *et al.* 2007; Bryant 2008). Modelling also shows that tsunami heights in the open ocean are directly proportional to the uplift of the seafloor above the source fault. Doubling that uplift (i.e. doubling the amount of slip on the fault plane) approximately doubles the peak-trough height of the tsunami. If we assume a ±15 per cent uncertainty in our earthquake source models, based on the signal recovered in our source inversion for the 2009 July 15 earthquake, related tsunami wave height uncertainties are ±0.05 m or less.

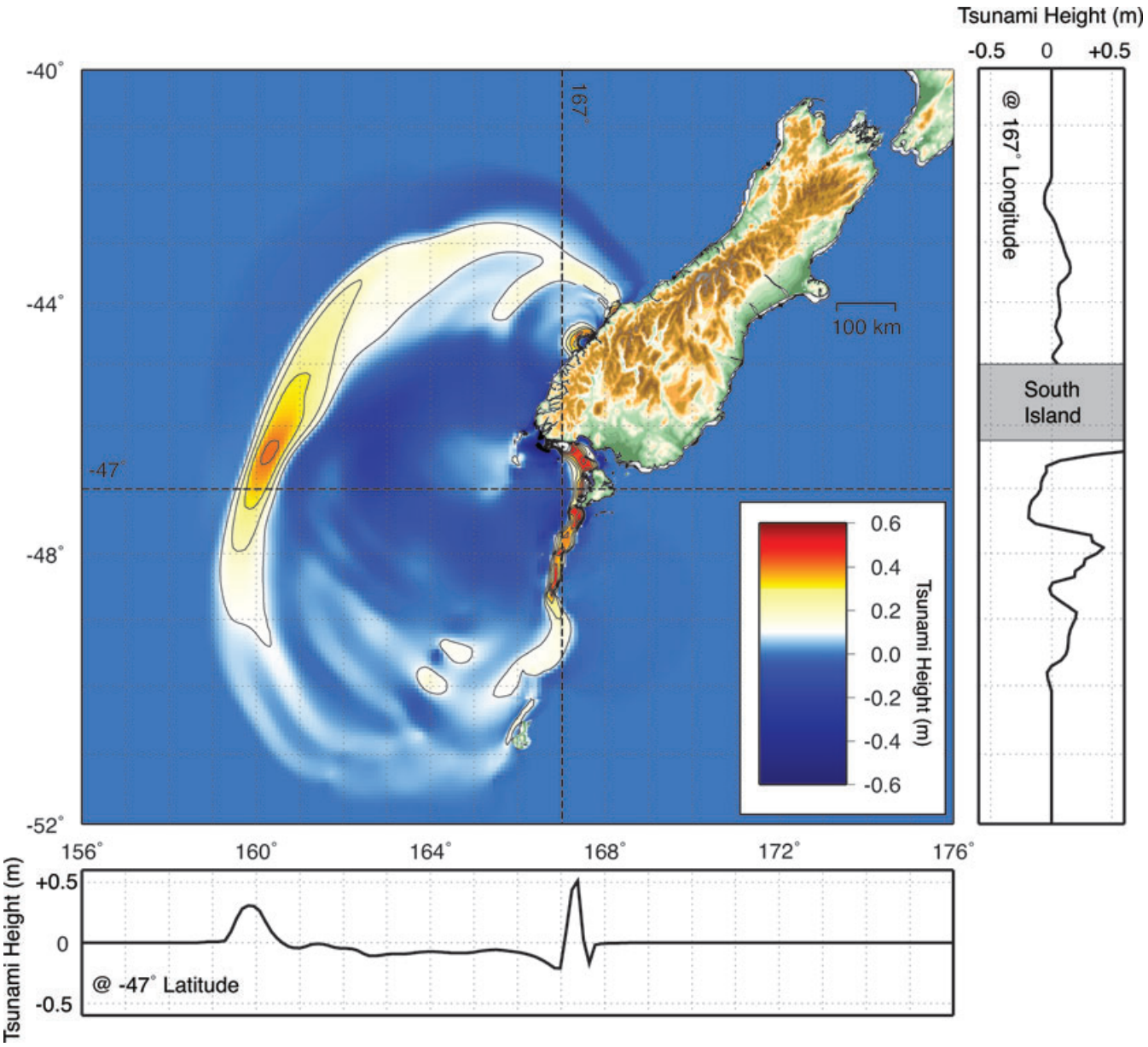

Figure 7. Tsunami amplitude 30 min after initiation. Light colours are positive heights, dark blues negative. Heights are contoured every 0.1 m, from 0.0 to 0.6 m. Panels at the base and left side are cross-sections through the tsunami at 47°S latitude, and 167°E longitude, respectively. Peak heights are located above the shallow continental shelf west of Stewart Island.

6 DISCUSSION AND CONCLUSIONS

Relatively small subduction zones like the Puysegur subduction zone, south of New Zealand can have a substantial tsunamigenic potential. Such subduction zones have generally been overlooked in past studies of global megathrust earthquake and tsunami potential, likely because of their size and relatively complex tectonic environments. However, even the relatively small Puysegur thrust interface is able to host $M > 8$ earthquakes, and thus also holds tsunami potential.

Our results show that the Puysegur subduction zone has tsunami generation potential that can affect New Zealand, Tasmania and the southeastern coast of Australia, and imply that this margin should be considered alongside other major convergent boundaries as being capable of megathrust seismogenesis and tsunami generation.

Perhaps more importantly, local and regional analyses of tsunami hazards rely on the recognition and accurate representation of causative earthquake hazards. Our analyses highlight that such hazards for the Puysegur subduction zone, and perhaps other similar convergent margins worldwide, have either been overlooked or have been recognized but treated without specific physical constraints. The tsunami potential of these margins should thus be revisited, such that additional locations of potential future tsunami sources can be identified, and plans for the dissemination of related hazards to the public, and warnings procedures in the event of their occurrence, be established.

ACKNOWLEDGMENTS

We thank Eric Geist and Daniel McNamara for comments and discussions during the preparation of this manuscript. We thank

Tuncay Taymaz and an anonymous reviewer for helpful comments related to the original version of this manuscript. Many of the figures were made using GMT, and we thank their developers and the users of their support list. We also thank Bob Engdahl and the Global Centroid Moment Tensor Group for the maintenance of and open access to their respective earthquake catalogues. Any use of trade, product or firm names is for descriptive purposes only and does not imply endorsement by the U.S. Government.

REFERENCES

Ammon, C.J., 2004. Relative earthquake location using surface waves, *EOS, Trans. Am. geophys. Un.*, **85**(47), Fall Meet. Suppl., Abstract S11B-1015.

Barnes, P.M., Sutherland, R. & Delteil, J., 2005. Strike-slip structure and sedimentary basins of the southern Alpine Fault, Fiordland, New Zealand, *GSA Bull.*, **117,** 411–435.

Bathgate, J.S., Volti, T. & Greenslade, D.J.M., 2008. The joint Australian tsunami warning centre: responding to a tsunamigenic earthquake—Puysegur Trench, 30 September 2007, *Preview, Australian Society of Exploration Geophysicists,* **133,** 40–44.

Berryman, K., 2005. Review of tsunami hazard and risk in New Zealand, *Institute of Geological & Nuclear Science*, *Client Report 2005/401*.

Bilham, R. & Ambraseys, N., 2005. Apparent Himalayan slip deficit from the summation of seismic moments for Himalayan earthquakes, 1500–2000, *Curr. Sci.,* **88,** 1658–1663.

Bryant, E., 2008. *Tsunami: The Underrated Hazard,* 2nd edn, Springer, New York, p. 330.

Cande, S.C. & Stock, J.M., 2004. Pacic-Antarctic–Australia motion and the formation of the Macquarie Plate, *Geophys. J. Int.,* **157,** 399–414.

DeMets, C., Gordon, R.G., Argus, D.F. & Stein, S., 1994. Effect of recent revisions to the geomagnetic reversal time scale on estimates of current plate motions, *Geophys. Res. Lett.,* **21,** 2191–2194.

Doser, D.I., Webb, T.H. & Maunder, D.E., 1999. Source parameters of large historical (1918–1962) earthquakes, South Island, New Zealand, *Geophys. J. Int.,* **139,** 769–794.

Downes, G. *et al*., 2005. EQC Project 03/490–Understanding local source tsunami: 1820s Southland tsunami, *Institute of Geological & Nuclear Science, Client Report 2005/.351*.

Engdahl, E.R. & Villaseñor, A., 2002. Global Seismicity: 1900–1999, in *International Handbook of Earthquake and Engineering Seismology, Part A,* Chapter 41, pp. 665–690, eds Lee, W.H.K., Kanamori, H., Jennings, P.C. & Kisslinger, C., Academic Press, London.

Engdahl, E.R., Van Der Hilst, R.D. & Buland, R.P., 1998. Global teleseismic earthquake relocation with improved travel times and procedures for depth determination, *Bull. seism. Soc. Am.,* **88,** 722–743.

Furlong, K.P., Lay, T. & Ammon, C.J., 2009. A great earthquake rupture across a rapidly evolving three-plate boundary, *Science,* **324,** 226–229.

Geist, E.L., Titov, V.V. & Synolakis, C.E., 2006. Tsunami: wave of change, *Sci. Am.,* **294,** 56–63.

González, F. I., Satake, K., Boss, E.F. & Mofjeld, H.O., 1995. Edge wave and non-trapped modes of the 25 April 1992 Cape Mendocino tsunami, *Pure appl. Geophys.,* **144,** 409–426.

Greenslade, D.J.M., Simanjuntak, M.A., Burbidge, D. & Chittleborough, J., 2007. A first-generation real-time tsunami forecasting system for the Australian region, *BMRC Research Report* **126**.

Greenslade, D.J.M., Simanjuntak, M.A. & Allen, S.C.R., 2009. An enhanced tsunami scenario database: T2, *CAWCR Technical Report* **14**.

Hayes, G.P., Furlong, K.P. & Ammon, C.J., 2009. Intraplate deformation adjacent to the Macquarie Ridge south of New Zealand—the tectonic evolution of a complex plate boundary, *Tectonophysics,* **463**, doi:10.1016/j.tecto.2008.09.024.

Ji, C., Wald, D.J. & Helmberger, D.V., 2002. Source description of the 1999 Hector Mine, California earthquake; Part I: wavelet domain inversion theory and resolution analysis, *Bull. seism. Soc. Am.,* **92,** 1192–1207.

Kajiura, K., 1986. Height distribution of the tsunami generated by the Nihonkai Chubu (Japan Sea Central Region) Earthquake, *Sci. Tsunami Haz.,* **4,** 3–14.

Lay, T., Kanamori, H. & Ruff, L., 1982. The asperity model and the nature of large subduction zone earthquakes, *Earthq. Predict. Res.,* **1,** 3–71.

Lebrun, J.-F., Lamarche, G. & Collot, J.-Y., 2003. Subduction initiation at a strike-slip plate boundary: the Cenozoic Pacific–Australian plate boundary, south of New Zealand, *J. geophys. Res.,* **108**. doi:10.1029/2002JB002041.

Lin, J. & Stein, R.S., 2004. Stress triggering in thrust and subduction earthquakes, and stress interaction between the southern San Andreas and nearby thrust and strike-slip faults, *J. geophys. Res.,* **109,** doi:10.1029/2003JB002607.

Lorito, S., Tiberti, M.M., Basili, R., Piatanesi, A. & Valensise, G., 2008. Earthquake-generated tsunamis in the Mediterranean Sea: scenarios of potential threats to Southern Italy, *J. geophys. Res.,* **113,** doi:10.1029/2007JB004943.

Malservisi, R., Furlong, K.P. & Anderson, H., 2003. Dynamic uplift in a transpressional regime: numerical model of the subduction area of Fiordland, New Zealand, *Earth planet Sci. Lett.,* **206,** 349–364.

McCaffrey, R., 2008. Global frequency of magnitude 9 earthquakes, *Geology,* **36,** 263–266.

McGinty, P. & Robinson, R., 2007. The 2003 M_w 7.2 Fiordland subduction earthquake, New Zealand: aftershock distribution, main shock fault plane and static stress changes on the overlying Alpine Fault, *Geophys. J. Int.,* **169,** 579–592.

Moore, M.A., Anderson, H.J. & Pearson, C., 2002. Seismic and geodetic constraints on plate boundary deformation across the northern Macquarie Ridge and southern South Island of New Zealand, *Geophys. J. Int.,* **143,** 847–880.

Pacheco, J.F., Sykes, L.R. & Scholz, C.H., 1993. Nature of seismic coupling along simple plate boundaries of the subduction type, *J. geophys. Res.* **98,** 14133–14159.

Peterson, E.T. & Seno, T., 1984. Factors affecting seismic moment release rates in subduction zones, *J. geophys. Res.* **89,** 10 233–10 248.

Power, W., Downes, G. & Stirling, M., 2007. Estimation of tsunami hazard in New Zealand due to South American earthquakes, *Pure appl. Geophys.* **164,** 547–564.

Reyners, M., Robinson, R., Pancha, A. & McGinty, P., 2003. Stresses and strains in a twisted subduction zone—Fiordland, New Zealand, *Geophys. J. Int.,* **148,** 637–648.

Sutherland, R., Barnes, P. & Uruski, C., 2006. Miocene—recent deformation, surface elevation, and volcanic intrusion of the overriding plate during subduction initiation, offshore southern Fiordland, Puysegur margin, southwest New Zealand, *New Zeal. J. Geol. Geophys.* **49,** 131–149.

Tichelaar, B.W. & Ruff, L.J., 1993. Depth of seismic coupling along subduction zones, *J. geophys. Res.* **98,** 2017–2037.

Toda, S., Stein, R.S., Richards-Dinger, K. & Bozkurt, S., 2005. Forecasting the evolution of seismicity in southern California: animations built on earthquake stress transfer, *J. geophys. Res.,* **110,** doi:10.1029/2004JB003415.

Wells, D.L. & Coppersmith, K.J., 1994. New empirical relationships among magnitude, rupture length, rupture width, rupture area, and surface displacement, *Bull. seism. Soc. Am.,* **84,** 974–1002.

Wells, R.E., Blakely, R.J., Sugiyama, Y., Scholl, D.W. & Dinterman, P.A., 2003. Basin-centered asperities in great subduction zone earthquakes: a link between slip, subsidence, and subduction erosion? *J. geophys. Res.* **108,** doi:10.1029/2002JB002072.

Yolsal, S., Taymaz, T. & Yalçiner, A.C., 2007. Understanding tsunamis, potential source regions and tsunami prone mechanisms in the Eastern Mediterranean, *Geological Society, London, Special Publications* **291,** 201–230.

SUPPORTING INFORMATION

Additional Supporting Information may be found in the online version of this article:

Figure S1. Conditions for slip partitioning along the Australia–Pacific Plate boundary through South Island, NZ. Plate motions (AUS, Australia; PAC, Pacific) are determined using the finite pole for anomaly 2Ay-present (∼2.58–0 Ma; Cande & Stock 2004). For the Alpine Fault location, Westland Terrain (WT) represents the region immediately east of the Alpine Fault. At that location slip partitioning is accomplished through deformation of the PAC Plate—for example shortening in the Southern Alps. Along the Fiordland segment of the plate boundary (FTT, Fiordland Trench Terrain, MS, Milford Sound), two possible slip-partitioning cases are shown. In both cases, motion along the Alpine fault segment is approximately 30 mm yr^{-1} (Barnes *et al.* 2005).

Figure S2. Surface deformation caused by the 2009 July 15 earthquake: (a) Horizontal and (b) vertical deformation, resulting from coseismic slip during the 2009 July 15 New Zealand earthquake (Fig. 3). The earthquake epicentre is marked with a red star. The black rectangle is the fault area of modelled coseismic slip, and the green rectangle outlines the area of major slip from Fig. 3. The AUS : PAC plate boundary is shown in red. Grey triangles mark the locations of three nearby GPS monuments of the permanent GNS Geonet network. In (a), black arrows indicate the scale and direction of horizontal deformation. In (b), colours describe surface uplift resulting from the earthquake: red = positive, blue = negative, contoured every 0.2 m.

Supplement. Details of historic tsunamis in southwest New Zealand, conditions for slip partitioning along the current plate boundary system, and surface deformation caused by the 2009 July 15 earthquake.

Movie. QuickTime animation of tsunami propagation through the Tasman Sea, based on our scenario earthquake model (Section 5).

Please note: Wiley-Blackwell are not responsible for the content or functionality of any supporting materials supplied by the authors. Any queries (other than missing material) should be directed to the corresponding author for the article.